Snow on Arctic sea ice in a warming climate as simulated in CESM2

M. A. Webster[1*], A. K. DuVivier[2], M. M. Holland[2], D. A. Bailey[2]

[1]University of Alaska Fairbanks, Geophysical Institute, 2156 Koyukuk Drive, Fairbanks, AK 99775, USA

[2]National Center for Atmospheric Research, 1850 Table Mesa Dr, Boulder, CO 80305, USA

*M. A. Webster, University of Alaska Fairbanks, Geophysical Institute, 2156 Koyukuk Drive, Fairbanks, AK 99775, USA (mwebster3@alaska.edu)

Key Points:

1. CESM2 (CESM-LE) snow depths are thinner (thicker) than observed snow depths.
2. The 1950-2050 trends in springtime snow depths on Arctic sea ice are -0.8 and -3.1 cm decade^{-1} in CESM2 and CESM-LE, respectively.
3. CESM2 shows enhanced earlier snowmelt, less snow accumulation, more sublimation, and slightly more snow-ice formation in future decades.

Plain Language Summary:

Snow on Arctic sea ice is important for several reasons: it creates a habitat for micro-organisms and mammals, it changes sea-ice growth and melt, and it affects the speed at which ships and people can travel over sea ice. Therefore, investigating how snow on Arctic sea ice may change in a warming climate is useful for anticipating its potential effects on ecosystems, sea ice, and socioeconomic activities. Here, we use experiments from the Community Earth System Model (CESM) to study how snow conditions change over time and between model versions. Observations show CESM2 underestimates snow depth and produces an overly-uniform snow distribution, while CESM1 produces excessively-thick, variable snow. The 1950-2050 trend in snow depth in CESM2 is 75% smaller than CESM1 due to CESM2 having less snow overall. Long-lasting, thick sea ice, cool summers, and excessive summer snowfall facilitate a thicker, longer-lasting snow cover in CESM1. In a warming climate, CESM2 shows that snow on Arctic sea ice will: (1) have greater, earlier spring melt, (2) accumulate less in summer-autumn, (3) sublimate more, and (4) cause marginally more snow-ice formation. CESM2 reveals that snow-free summers can occur ~30-60 years before an ice-free central Arctic, which may promote faster sea-ice melt.

Abstract:

Earth system models are valuable tools for understanding how the Arctic snow-ice system may respond to a warming climate and the feedbacks therein. In this analysis, we investigate snow on Arctic sea ice to better understand how snow conditions may change under different forcing scenarios. First, we use *in situ*, airborne, and satellite observations to assess the realism of the Community Earth System Model (CESM) in simulating snow on Arctic sea ice. CESM Versions 1 and 2 are evaluated, with V1 being the Large Ensemble experiment (CESM-LE) and two configurations of V2 with low- and high-top atmospheric components. The assessment shows CESM2 underestimates snow depth and produces overly-uniform snow distributions, whereas CESM-LE produces an excessively-thick, highly-variable snow cover. Observations indicate that snow in CESM2 accumulates too slowly in autumn, too quickly in winter-spring, and melts too soon and rapidly in late spring. The 1950-2050 trends in springtime snow depths are markedly smaller in CESM2 (-0.8 cm decade^{-1}) than in CESM-LE (-3.1 cm decade^{-1}) due to CESM2 having less snow overall. A perennial, thick sea-ice cover, cool summers, and excessive summer snowfall facilitate a thicker, longer-lasting snow cover in CESM-LE. Under the SSP5-8.5 forcing scenario, CESM2 shows that, compared to present-day, snow on Arctic sea ice will: (1) undergo enhanced, earlier spring melt, (2) accumulate less in summer-autumn, (3) sublimate more, and (4) facilitate marginally more snow-ice formation. CESM2 also reveals that snow-free summers can occur ~30-60 years before an ice-free central Arctic, which may promote faster sea-ice melt.

1. Introduction

Snow is an integral part of the Arctic sea-ice and climate systems, having both positive and negative effects on sea-ice mass balance (*Sturm and Massom,* 2017; *Webster et al.,* 2018). Snow's reflectivity is important for maintaining a high surface albedo on sea ice during spring and summer (*Perovich et al.,* 2002; *Perovich and Polashenski,* 2012; *Holland and Landrum,* 2015), which can delay sea-ice surface melt and melt pond formation (*Petrich et al.,* 2012; *Webster et al.,* 2015; *Perovich et al.,* 2017a). During sea-ice formation, snow is an effective insulator that limits ocean heat flux through sea ice to the atmosphere, thereby hindering sea-ice growth rates (*Maykut,* 1978; *Sturm et al.,* 2002). In some cases, a deep snowpack is sufficiently heavy to depress the sea-ice surface into the ocean, allowing seawater to flood the snow and freeze (*Provost et al.,* 2017). These are just some of the snow processes that modify the Arctic sea-ice mass balance (*Sturm and Massom,* 2017). With respect to a warming Arctic climate, questions arise as to how snow processes and conditions will be affected, and whether these changes will fundamentally change the role of snow in the Arctic sea-ice system.

Earth system models are valuable tools for understanding how the snow-ice system may respond to a warming climate. Earlier modeling efforts (*Hezel et al.,* 2012; *Blanchard-Wrigglesworth et al.,* 2015) have projected a decline in snow thickness on Arctic sea ice owing to later sea-ice formation in autumn, an increasing ratio of liquid-to-solid precipitation, and transition from a perennial to seasonal sea-ice cover. In the western Arctic, these projections have been corroborated by observations showing a decrease in spring snow related to later sea-ice formation in autumn (*Webster et al.,* 2014). Although models show a projected increase in snowfall during winter, which could facilitate a thicker snow cover, the models show a decline in the annual mean snowfall as the Arctic transitions to a rain-dominated summer and autumn

(*Holland et al.,* 2007; *Lique et al.,* 2016; *Bintanja and Andry,* 2017). Such changes in precipitation and the concomitant changes in sea-ice conditions will affect whether snow has a net positive or negative effect on sea-ice mass balance by way of governing which snow processes dominate. As an example, increased snowfall over thin sea ice may lead to more widespread snow-ice formation, which would act as a negative feedback in sea-ice mass balance.

In this study, we investigate the changes in snow's role in the Arctic sea-ice system under anthropogenic warming using ensemble simulations from two versions of the Community Earth System Model (CESM). For the first time, projections of snow-on-sea ice processes are quantified and related to changes in sea-ice conditions and precipitation in an Earth system model. Snow thickness distributions are evaluated on temporal and spatial perspectives, and assessed using a synthesis of *in situ*, airborne, and satellite data. The main findings of this analysis provide new information on the rate of change in snow conditions on sea ice across Arctic basins, which snow processes dominate in different climate states, and the atmospheric and sea-ice conditions that may modify snow's role in the changing Arctic sea-ice system.

2. Data and Methods

The primary data sets of the analysis are freely available CESM output, supplemented by field, airborne, and satellite observations of snow and freeboard conditions.

2.1 CESM-LE and CESM2

CESM output from multiple model experiments was analyzed to understand projections of snow conditions on sea ice in a warming climate. We evaluate ensemble simulations from three CESM configurations: (1) CESM Version 1 with the CAM5 atmospheric component

(*Hurrell et al.,* 2013) performed as part of the CESM Large Ensemble (CESM-LE) Project (*Kay et al.,* 2015), and CESM Version 2 (*Danabasoglu et al.,* 2020) with the (2) CAM6 atmospheric component and (3) WACCM6 (*Gettelman et al.,* 2019) atmospheric component. To briefly summarize, the major differences between the CAM6 and WACCM6 atmospheric models are the location of the model top (at 40 km in CAM6 and 140 km in WACCM6) and the presence of prognostic chemistry in WACCM6. The CAM6 and WACCM6 use the same physics and horizontal resolution. For more details between atmospheric components, we refer readers to *Danabasoglu et al.,* (2020) and *Gettelman et al.* (2019).

The sea ice component in CESM2 uses the Los Alamos Sea Ice Model (CICE5; *Hunke et al.,* 2015). This is a dynamic-thermodynamic model which utilizes the elastic-viscous-plastic dynamics (*Hunke and Dukowicz,* 2002) and incorporates a sub-grid-scale ice thickness distribution. Relative to CESM-LE, which used the earlier CICE4 model version (*Hunke and Lipscomb,* 2008) with some updates (*Holland et al.,* 2012), the new CICE5 model simulates sea ice as a mushy layer and incorporates prognostic salinity (*Turner et al.,* 2013; *Hunke et al.,* 2015; *D. Bailey et al.,* personal communication, 2020). The melt pond formulation is also updated to better reflect differences in ponding on level ice (*Hunke et al.,* 2013). Aspects of Arctic sea ice conditions as simulated by CESM2 are discussed in *DuVivier et al.* (submitted) and *DeRepentigny et al.* (submitted).

For the CESM-LE, we analyze output for the 1920-2100 time period. Each model configuration and experiment had a different number of ensemble members available (**Table 1**), which should be considered when interpreting the results. The long-term changes in snow conditions were analyzed primarily using results from the RCP8.5 forcing scenario (*van Vuuren et al.,* 2011) for CESM-LE and the SSP5-8.5 forcing scenario (*O'Neill et al.,* 2016) for CESM2.

While these are driven with somewhat different forcing scenarios, they have a similar radiative forcing by the end of the 21st century and, thus, are roughly comparable. Even so, the CESM-LE with RCP8.5 reaches a higher global mean temperature by 2100 compared to the CESM2 SSP5-8.5 simulations (*Meehl et al.*, submitted), with consequences for Arctic sea ice loss (*DeRepentigny et al.*, submitted).

Using CESM2 output, we also evaluate the projections of snow on Arctic sea ice under four different forcing scenarios: SSP1-2.6, SSP2-4.5, SSP3-7.0, and SSP5-8.5. They can be summarized as scenarios with low, medium, medium-to-high, and high radiative forcing conditions and differing shared socioeconomic pathways. Details about these scenarios can be found in *O-Neill et al.* (2016).

Snow depth on sea ice is analyzed in model grid cells where the sea ice concentration is 15% and greater. In the trend analyses, all values reported have 99% statistical significance. For determining the duration of the snow cover, grid cells with at least 0.01 m of snow and 15% sea ice concentration are counted. We define the duration as the number of days that meet the criteria, regardless of temporal continuity. To explore the relationship between snow-free and ice-free conditions, we compare dates at which these conditions occur in the 80°N-90°N region of the central Arctic. We define ice-free conditions as less than 1 million km^2 in sea ice area and snow-free conditions as a monthly mean snow depth value of 0.01 m or less.

We evaluate five snow processes that constitute the snow mass budget: (1) mass gain from snowfall, (2) mass gain and loss from condensation and sublimation, respectively, (3) mass loss from snowmelt, (4) mass loss from snow-ice formation, and (5) mass change from sea-ice dynamics, which is treated as a residual term in the snow mass budget. The total snow mass is calculated as the difference between the first and last day's snow depth of a given month,

converted to units of cm day^{-1}. A spatial mask of 80ºN-90ºN is applied to mitigate the effects of sea-ice loss on the snow mass budget terms. The 80ºN-90ºN region also isolates the same set of model grid cells where sea ice is predominantly present across model ensemble members and decades for each month. In this way, we are able to evaluate changes in snow processes due to feedbacks within the Arctic system (e.g., less snowfall), rather than have the decreasingly extensive sea-ice cover imprinted on any diagnosed snow trends.

2.2 Field, Airborne, and Satellite Data

Four "observational" data sets are used to assess the temporal and spatial aspects of snow depth on Arctic sea ice from CESM-LE and CESM2 (**Table 2**). These include ground, buoy, airborne, and satellite data.

2.2.1 Field Observations

For examining the seasonal cycle of snow, monthly snow depths were co-located and compared with those measured *in situ* at the North Pole drifting ice stations in 1954-1991 (*Radionov et al.,* 1997) and derived from drifting ice mass balance (IMB) buoys in 1997-2017 (*Perovich et al.,* 2017b). The North Pole drifting ice stations encompassed the central and eastern Arctic, whereas the IMBs were mostly located in the central and western Arctic (**Supplementary Figure 1**). The two periods between data sets represent historical and contemporary sea-ice conditions, although we note earlier work showed no statistical difference in snow accumulation rates between the station and IMB data (*Webster et al.,* 2014). A total of 64 IMBs from 1997-2017 are analyzed, yielding an average of 1,369 individual recordings per month, a minimum of 907 in February, and maximum of 1,654 in October. We omit comparisons with the ice station

178 data in summer due to ground measurements ceasing when snow covered less than 50% of the
179 survey lines or when average snow depths were less than 5 cm in thickness (*Radionov et al.*,
180 1997; *Warren et al.*, 1999), which would create a high bias in the summer station data.
181
182 **2.2.1 Airborne Data**
183 We assess the spatial distribution of modeled snow depths for March-April using airborne
184 data. Snow thickness is derived from measurements from the University of Kansas' ultra-
185 wideband microwave radar on NASA's Operation IceBridge mission (*Koenig et al.*, 2010;
186 *Panzer et al.*, 2010; *Kwok et al.*, 2011). The spatial assessment using airborne data is limited to
187 western longitudes due to absence of airborne surveys in the eastern Arctic. We compare
188 averages between the modeled and observed snow depths in grid cells where at least 100
189 airborne measurements were collected. The airborne data do not include snow-free surfaces and
190 therefore may be biased high. Another source of bias may be the effects of saline snow, which
191 can cause a shallower detection of the assumed snow-ice interface and thus underestimate snow
192 depth (*Nanden et al.*, 2017).
193
194 **2.2.3 Satellite Data**
195 Due to the limitation of ground and airborne observations both in space (i.e. western
196 Arctic) and time (spring season), we use data from NASA's Ice, Cloud, and land Elevation
197 Satellite 2 (ICESat-2) mission to derive and examine a full annual cycle of snow depth
198 distributions across the entire Arctic basin. ICESat-2's laser altimeter theoretically detects the
199 surface of the snow-covered (or snow-free) sea ice, and, using a reference sea level height and
200 assumed densities, total freeboard is determined (*Kwok et al.*, 2019). The difference between the

total (snow and ice) freeboard and sea-ice freeboard theoretically yields snow depth (**Figure 1**). Since snow and ice densities and sea ice thickness values are known in CESM, we can use them with ICESat-2 total freeboards to infer snow depth.

Assuming hydrostatic balance for sea ice, snow depth (h_s) can be solved for as in *Kwok et al.* (in review):

$$h_s = \frac{\rho_w}{\rho_w - \rho_s} f_t - \frac{\rho_w - \rho_i}{\rho_w - \rho_s} h_i \quad (1)$$

where h_i is sea ice thickness (from CESM), ρ_w is the density of seawater, ρ_s is the density of snow, ρ_i is the density of sea ice, and f_t is the total freeboard (from ICESat-2). Density values of snow and sea ice - 330 kg m^{-3} and 917 kg m^{-3}, respectively - are fixed in the model. Seawater density is not held constant in CESM; however, we assumed a seawater density of 1026 kg m^{-3} for our calculations, which is commonly used value in the altimetry community (e.g. *Kwok et al.*, 2020). The along-track freeboard product (*Kwok et al.*, 2019) was gridded to the same resolution of the CESM data and used to derive a synthesized snow depth estimate for October 2018 – September 2019. We note a month-long data gap in mid-June to mid-July 2019 due to a software error putting ICESat-2 into safety mode.

The inferred snow depths were compared with those directly available from CESM to investigate possible seasonal and regional biases in snow depth distributions. We use monthly means of sea ice thickness for 2010-2019 to infer snow depth. The 2010-2019 period was chosen due to the temporal overlap with ICESat-2 data and good agreement of mean sea-ice extent in CESM2 with the passive microwave observations in 2018-2019 (*Fetterer et al.*, 2017) (**Supplementary Figure 2**).

3. Results and Discussion

We first present the spatial and temporal assessments of simulated snow depths from comparisons with *in situ*, buoy, airborne, and satellite data. The second component of the analysis describes the long-term changes in snow depth under different forcing scenarios for CESM-LE and CESM2. The third component of this paper describes the changes in the seasonal cycle of snow in relation to sea-ice conditions. The final component presents the decadal changes in the snow mass budget, how the budgets differ between models, and the general spatial distribution of snow processes over time.

3.1 Comparison with observations

3.1.1 Spatial distribution

The modeled snow depths for the spring season exhibit a similar spatial pattern of Arctic snow across all model configurations: deep snow is found north of Greenland and the Canadian Archipelago and thinner snow is predominantly located in the peripheral seas (**Figure 2**). An exception to this pattern is the exceptionally deep snow (i.e. greater than one meter) directly east of Greenland in the CESM-LE. Qualitatively, the cross-basin distribution of snow is consistent with ground and airborne observations; however, the range in snow depth differs. Snow depths in CESM-LE were thicker and distributed more heterogeneously than the airborne observations, with snow depths being greater than one meter in places (**Figure 3**). CESM-LE exhibited a bimodal snow depth distribution similar to that in the Operation IceBridge retrievals. The timing of sea-ice freeze-up and age of sea ice create this bimodal distribution; first-year sea ice has less time to accumulate snow and therefore tends to have thinner snow conditions than multiyear sea

ice in this region (*Kurtz and Farrell,* 2011; *Webster et al.,* 2014). The bimodal distribution is not captured in CESM2, and snow depths in both CAM6 and WACCM6 are thinner and more uniform than the airborne observations and CESM-LE. The largest discrepancy occurs north of Greenland (i.e. Lincoln Sea region), where CESM2 snow depths are ~10-20 cm thinner than the airborne observations. Interestingly, CESM2-WACCM6 has a more uniform snow depth distribution than CESM2-CAM6, despite having greater variability and a larger range in sea ice thickness along the Operation IceBridge survey lines (**Supplementary Figure 3**).

3.1.2 Seasonal cycle

The comparisons of CESM2 snow depths with *in situ*, buoy, and satellite data suggest three important findings for the simulated seasonal cycle (**Figure 4**). CESM2-CAM6 and WACCM6 appear to: (1) underestimate snow accumulation and depth in autumn, (2) overestimate the rate of snow accumulation in late winter and early spring, and (3) melt snow too early and too rapidly from late spring into early summer. For CESM-LE, the results were in mixed agreement with the observations. Here, we describe the evaluation of the seasonal cycle, starting with point measurements, scaling up to ground surveys 500 m – 1000 m in length, and concluding with a back-of-the-envelope assessment using satellite data.

In situ and buoy comparisons:

We start with the CESM2 analysis at the start of the snow accumulation season in August, when snow depths increase from their minimum values (**Figure 4**). Note, the ice station (1954-1991: historic) and IMB (1997-2017: contemporary) data represent different time periods. In August – November, snow accumulates rapidly at the IMBs and ice stations, with IMBs

having slightly larger accumulation rates. The buildup of the snowpack in CESM2-CAM6 and WACCM6 was approximately half (~2 cm $month^{-1}$) the rate recorded by the IMBs (~5 cm $month^{-1}$) and at the drifting ice stations (~4 cm $month^{-1}$). From January to May, CESM2 gains more snow (~2 cm $month^{-1}$) than both the IMBs (~-1 cm $month^{-1}$) and ice stations (~1 cm $month^{-1}$).

During the early melt season, the observations and models exhibit disparate snowmelt onset dates and rates. In CESM2, a dramatic decline in snow depth began in May, while the snowmelt rates recorded by the IMBs and at the stations were most extreme in June. CESM2 exhibited snow-free conditions earlier than the IMBs (July vs. August), which has important implications for a positive albedo feedback. By and large, CESM2 snow depths were thinner than the drifting ice station data, but produce a representative seasonal cycle for the 1954-1991 period. In contrast, the modeled seasonal cycle of the 1997-2017 period has poor agreement with the IMB data, although this relationship likely worsens due to the large heterogeneity in point IMB measurements relative to mean values of model grid cells and ground survey lines.

The CESM-LE snow depths had considerably larger variability at the IMB and ice station locations than CESM2, which should be considered when interpreting the following results. The autumn accumulation rate in CESM-LE compares well with the ice stations observations, but the accumulation rate for the contemporary period is ~2 cm $month^{-1}$ smaller than the IMB observations. From January to May, snow accumulation rates diverge between the historic and contemporary periods. Both CESM-LE and ice station accumulation rates were ~1 cm $month^{-1}$, whereas rates in the contemporary period were ~2 cm $month^{-1}$ greater than the IMB observations. In summer, both CESM-LE and the ice stations exhibited the same melt rate of -8 cm $month^{-1}$. At the IMB sites, the melt rate in CESM-LE was double the IMB observations (~-8

293 cm vs. -4 cm month^{-1}). In short, CESM-LE has good agreement with the observations relative to
294 CESM2, better simulates the historic seasonal cycle, but poorly captures the seasonal cycle for
295 the contemporary period.
296
297 *Satellite comparison:*
298 To assess the full annual cycle of snow depth distributions across the entire Arctic basin,
299 we compared modeled snow depths with inferred snow depth using ICESat-2 total freeboard data
300 and simulated sea-ice thicknesses (**Figure 5**). Such a comparison gives greater insight into the
301 unique geographic differences of snow conditions between Arctic regions. While the inferred
302 snow depths from ICESat-2 show greater spatial variability than the CESM2 snow depths (not
303 shown), the ICESat-2 data are from 2018-2019 and the model data are an average over 2010-
304 2019. As a consequence, there may be interannual climate variability muddying the signal. The
305 results shown in **Figure 5** were derived from CESM2-WACCM6 data and comparable to those
306 produced using CESM2-CAM6 data (**Supplementary 4)**.
307 We find that the comparison between the modeled and inferred snow depths show the
308 same general differences as those with the IMB and station data (**Figure 4**). During the autumn
309 buildup of the snowpack, CESM2 appears to underestimate snow depth relative to the inferred
310 snow depths in most Arctic regions. CESM2 tends to underestimate sea-ice thickness in autumn,
311 particularly in areas with multiyear ice (i.e. Lincoln Sea and southern Beaufort and Chukchi
312 seas) (*DuVivier et al.*, submitted). As a consequence, a low bias in sea-ice thickness increases the
313 inferred snow depths (Equation 1) and may contribute to the discrepancy in autumn snow depths.
314 Comparing the ICESat-2 and CESM2 total (snow and sea ice) freeboards, we find CESM2 total

freeboards to be smaller than the satellite observations nearly year-round except for July and August (**Supplementary Figure 5**).

From December to June, both the accumulation rates and snow depths in CESM2 markedly exceed the inferred snow depth in the eastern Arctic, which is consistent with the comparisons with the IMB and ice station data. With the exception of a small portion in the northern Chukchi Sea and the southern Lincoln Sea (i.e. multiyear ice areas), CESM2 snow depths are thicker than the inferred snow depths across all Arctic basins prior to melt onset. In May – June, the peak in snowmelt occurs in both CESM2 and the inferred snow depths, with CESM2 losing ~40 cm of snow in some locations. While CESM2 shows better agreement with sea-ice thickness observations in spring (see Figure 5 in *DuVivier et al.,* 2020), the total (snow and sea ice) freeboard comparisons show large discrepancies with CESM2 having predominantly larger total freeboards than the ICESat-2 data (**Supplementary Figure 5**).

The results in Figure 4 show strong spatial heterogeneity between Arctic regions, as well as the inter-annual variability in atmosphere-snow-ice conditions imprinted on the ICESat-2 data. For example, the feature in the northern Chukchi Sea in March and April has an inferred snow depth ~10-20 cm deeper than that in CESM2. Given that a monthly ensemble mean from CESM2 is used to infer snow depth (Equation 1), the source of this feature is the locally-large, total freeboard values in ICESat-2 data. In *Kwok et al.,* (2020), this particular feature was attributed to deep snow from anomalously high cyclone activity and cyclone-associated snowfall over sea ice in the northern Chukchi Sea during the 2018-2019 snow accumulation season relative to the 1979-2019 cyclone climatology (*Webster et al.,* 2019).

3.2 Long-term changes

3.2.1 Coverage

Snow depth on Arctic sea ice declines under all forcing scenarios over 1950-2050 in CESM2-CAM6 and WACCM6 (**Figure 6**). The 1950-2050 trends range from -0.5 cm per decade (SSP3-7.0) to -0.7 cm per decade (SSP5-8.5). Interestingly, the SSP3-7.0 forcing scenario produces the smallest trend of all forcing scenarios, despite having higher radiative forcing, a stronger global forcing pathway, and a larger shared socioeconomic pathway than the SSP1-2.6 and SSP2-4.5 forcing scenarios. Beyond 2050, the annual mean snow depths have stronger correspondence to the forcing scenarios, with the deepest snow cover occurring under the weakest forcing scenario (SSP1-2.6) and the thinnest snow cover occurring under the strongest forcing scenarios (SSP5-8.5).

As evidenced in Figures 1 and 2, snow conditions between CESM-LE and CESM2 are strikingly different. The annual mean snow depth in the CESM-LE (for 80ºN-90ºN) is approximately twice as thick as that in CESM2-CAM6 and CESM2-WACCM6 for the 1920-2100 period (**Figure 7a**). The trends over 1950-2050 also show marked differences between model configurations. The annual mean in snow depth declines at -3.6 cm decade^{-1} in CESM-LE, whereas the trends in CESM2-CAM6 and WACCM6 are notably more gradual at -0.8 cm decade^{-1}. The observed trend, which is limited to the 1954-2013 March-April season only, was -2.9 cm decade^{-1} (*Webster et al.*, 2014). Comparatively, we find that the 1954-2013 March-April trend in CESM-LE (-2.9 cm decade^{-1}) shows strong agreement with the observed trend, while trends in CESM2 are considerably smaller (-0.4 to -0.5 cm decade^{-1}). The discrepancy in trends between model versions may be partly explained by the thinner snow depth conditions in CESM2 for the earlier part of its simulated record (**Figure 7a**).

The snow cover in CESM-LE was more persistent throughout the 1920-2100 period than that in CESM2 (**Figures 7b and 8**). This can be attributed in part to greater coverage and persistence of sea ice (*DeRepentigny et al.,* submitted) as well as to excessive snowfall and cooler summers in CESM-LE (*McIlhattan et al.,* 2017; *McIlhattan et al.,* submitted), which helps retain a high surface albedo and consequently promotes a negative albedo feedback (*Light et al.,* 2015). In contrast, Arctic sea ice is less extensive and the snowfall rate decreased slightly in CESM2-CAM6, and both CAM6 and WACCM6 exhibit later sea-ice formation than CESM-LE (*DeRepentigny et al.,* submitted; *McIllhatten et al.,* submitted). When comparing CESM2 atmospheric components, both the snow and sea-ice covers in CESM2-WACCM6 survive longer during the summer melt season than those in CESM2-CAM6 (**Figure 7b and Supplementary Figure 6**). As shown in *DuVivier et al.* (submitted), CAM6 has more incoming shortwave radiation, which may promote earlier, faster melt of the snow cover and facilitate a stronger positive albedo feedback. The largest differences in snow cover duration occur in the peripheral seas (**Figure 8**), with the Chukchi and Kara seas exhibiting differences of more than 50 days. As shown in Figures 3 and 5 in *DuVivier et al.* (submitted), sea ice is considerably thinner and less extensive in CESM2-CAM6 than CESM2-WACCM6 in these peripheral seas.

3.2.2 Seasonality

Across all CESM configurations, the snow depth minimum occurs in mid-August, nearly a month before the sea ice minimum extent in September (**Figures 8, a**). This suggests that, while new snow may accumulate in mid-summer, the albedo impact is not sufficient to halt summer ice melt and that other factors such as bottom melt sustain summer ice loss through to mid-September. This is further supported by the prolonged decrease in sea ice thickness after the

snow depth minimum (**Figure 9, c**). The snow depth maximum occurs at similar times across all model configurations; however, peak snowmelt is distinctly earlier in CESM2 than CESM-LE in the 1950s and 2000s. *DuVivier et al.,* (2020) found that CESM2-CAM6 exhibits earlier, stronger melt than CESM2-WACCM6 due to fewer clouds, which subsequently allows greater shortwave radiation at the surface. By the 2050s, peak melt is concurrent across all model configurations.

In general, CESM-LE produces more annual snowfall than CESM2 over 80-90ºN (**Figure 9, d and Figure 10, a**). The largest differences occur in June – August (~2-4 mm month^{-1}), when freshly accumulated snow has the largest effect in increasing surface albedo (**Figure 10, b**) (*Holland and Landrum,* 2015; *Light et al.,* 2015). Although the 1920-2100 trends in snowfall for CESM-LE and CESM2-WACCM6 are similar (3.3 and 3.1 mm decade^{-1}, respectively), CESM-LE has considerably higher snowfall (+20 mm) at the beginning of the time-series. CESM2-CAM6 also produces less snowfall than CESM-LE for the earlier part of the series, but its snowfall increases by 4.5 mm decade^{-1} and surpasses CESM-LE snowfall by 2100 (**Figure 10, a**). The comparison between CESM2-CAM6 and WACCM6 reveals that CAM6 has more annual snowfall than WACCM6 for 1920-2100, averaging 196 vs. 187 mm. However, WACCM6 has more snowfall during the summer melt season of ~2-3 mm month^{-1} (**Figure 10, b**), which may help reduce sea-ice surface melt.

Snow-free summers (mean snow depth value of 0.01 m or less in 80ºN-90ºN) become an emerging feature in the 1930s for CESM2-CAM6 and 2000s for WACCM6, whereas the first snow-free summer occurs in the 2040s in CESM-LE (**Figure 11**). In CESM2, thin snow (i.e. less than 3 cm) occurs throughout the historical runs in summer, which may be related to less perennial sea ice in CESM2 relative to CESM-LE (*DeRepentigny et al.*, submitted), as well as the warmer summer temperatures in CESM2-CAM6 (*McIllhatten et al.*, submitted). In context of

sea-ice retreat, ice-free summers (less than 1 million km^2 covering 80ºN-90ºN) first occur in the 2020s, 2030s, and 2040s for CESM2-CAM6, CESM2-WACCM6, and CESM-LE, respectively. These results indicate that while the loss of snow is a reinforcing factor in the positive albedo feedback (*Holland and Landrum,* 2015), snow-free summers can persist for ~30-60 years before the onset of an ice-free central Arctic in CESM2. In CESM-LE, the first snow-free and ice-free summers occur within the same decade.

3.3 Snow processes

Under the SSP5-8.5 forcing scenario, the 1950s – 2050s decadal changes in the snow mass budgets of WACCM6 and CAM6 reveal: (1) greater, earlier spring melt, (2) less snow accumulation in late summer and early autumn, (3) slightly enhanced winter snow accumulation in WACCM6, but less winter accumulation in CAM6, (4) less condensation and more sublimation, and (5) a marginal increase in snow-ice formation (**Figures 12-13**).

The largest sink in the snow mass budget is snowmelt. Snowmelt in spring was more than three times greater in the 2050s than in the 1950s in WACCM6, and doubled in the 2050s in CAM6 (**Figures 12, c-d and 12**). In the 2000s and 2050s, snowmelt in July – September decreases due to the absence of snow and sea ice. Snow accumulation rates in WACCM6 decreased by ~88% in August – October by the 2050s largely due to sea-ice loss, but increased by ~31% in December – February. In contrast, snow accumulation in CAM6 decreased in all months, with a 64% decrease in the annual total (**Figure 12, e-f**), despite the increase in annual snowfall (**Figure 10, a)**. Although sublimation and condensation play very small roles in the snow mass budget, we found an overall shift from condensation (positive mass contribution) to sublimation (negative mass contribution) (**Figure 12, a-b**) between the 1950s and 2050s.

As sea ice thins and snowfall increases, sea ice may become more susceptible to snow-ice formation if snow accumulation rates are sufficiently large. We found rates of snow-ice formation decreased by ~0.01 to 0.03 cm day^{-1} in September – October in both CESM2 model configurations between the 1950s and 2050s (**Figure 12, g-h**). We attribute this decrease due to the absence of sea ice, which forms progressing later during the 21st century (**Figure 9, b**). In contrast, snow-ice formation in January – April increases by ~0.01-0.02 cm day^{-1}, which may correspond with thinner sea ice (**Figures 9, c**) and more snowfall (**Figure 10, a**). Despite the seasonal changes in snow-ice formation rates, its contribution to the snow mass budget remains small in all future decades under the RCP 8.5 and SSP5-8.5 forcing scenarios (**Figures 12-13, and Supplementary Figure 7**). This result indicates that the snow-ice system maintains a sufficiently high ratio of sea ice-to-snow thickness to preclude widespread snow-ice formation in current and future decades.

Regarding the spatial distribution of snow processes, similar patterns emerge between specific snow conditions and atmosphere-snow-ice interactions. In the 2000s, the mass gain from snowfall is largest in the northern Atlantic Ocean and Bering Sea, where the north Atlantic and north Pacific storm tracks intersect with the Arctic (**Figure 14**). These areas also coincide with thinner sea ice (see Figure 5 in *DuVivier et al.*, submitted), early season bottom sea-ice melt (**Supplementary Figure 8**), and a greater prevalence of snow loss due to snow-ice formation in CAM6 (not shown) and WACCM6 (**Figure 14**). As future models improve in spatial resolution and treatment of physics, greater understanding can be gleaned of the governing mechanisms from such regional differences in the snow-sea ice system.

4. Conclusions

452 In this study, we use climate model experiments to investigate how snow conditions on
453 Arctic sea ice may respond to a warming climate. We evaluated Versions 1 and 2 of CESM using
454 *in situ*, airborne, and satellite observations. The assessment shows that CESM2-CAM6 and
455 WACCM6 produce a snow cover that is too thin and too uniform, whereas snow in CESM-LE is
456 excessively thick and heterogeneous. Snow in all model configurations thins in a warming
457 climate; however, the 1950-2050 trend in CESM2 is 75% smaller than that in CESM-LE owing
458 to thinner snow in CESM2 throughout 1850-2100.

459 The differences in the mean sea-ice state and precipitation are the primary contributing
460 factors to dissimilar snow conditions between model configurations. For example, the combined
461 effect of a perennial, thick sea-ice cover, cool summers, and excessive summer snowfall in
462 CESM-LE facilitates a thicker, longer-lasting snow cover relative to snow in CESM2. These
463 results highlight the importance of the strong coupling between snow, sea-ice, and atmospheric
464 conditions (*Webster et al.,* 2018), which manifests in the trends of snow depth under the RCP8.5
465 forcing scenario between model configurations.

466 All model configurations show similar seasonal changes in the following snow processes
467 for future projections:

468 1. Earlier, enhanced snow melt in spring;

469 2. Less snow accumulation in summer and early autumn;

470 3. More sublimation year-round; and

471 4. Slightly more snow-ice formation.

472 These changes have important implications for climate feedbacks and the sea-ice mass
473 budgets in the Arctic. An earlier spring melt (process 1) would promote a positive albedo
474 feedback and enhance sea-ice melt. Less summer snow accumulation (process 2) would also

475 create a positive albedo feedback; however, since this impacts late summer when solar insolation
476 is low, its influence would be reduced relative to the earlier spring melt. Perhaps more
477 importantly, less snow in autumn as sea ice is beginning to form would allow sea ice to grow
478 faster due to a reduction in the snow's insulating effect. To better understand the net effects of
479 these projected snow changes for the ice mass budgets and climate feedbacks, model
480 experiments with prescribed snow changes would be useful and will be pursued in future work.
481 It is uncertain what the effects of greater sublimation (process 3) will have on the
482 atmospheric state, but more may be learned from the recent observations from the
483 Multidisciplinary drifting Observatory for the Study of Arctic Climate (MOSAiC) expedition
484 and using such observations to guide accompanying model experiments. While snow-ice
485 formation increases (process 4), it still has a negligible contribution to the total Arctic snow mass
486 budget. However, there may be specific regions where this process becomes increasingly
487 important over time, such as Bering Strait and Fram Strait (**Figure 14**). Combined modeling and
488 observational efforts could progress the science and understanding of the atmosphere-snow-ice
489 interactions unique to these (and other) regions, especially in light of testing improved physics
490 and resolutions in ongoing model development.
491
492
493
494 **Acknowledgements**
495 The CESM project is supported primarily by the National Science Foundation (NSF). This
496 material is based upon work supported by the National Center for Atmospheric Research
497 (NCAR), which is a major facility sponsored by the NSF under Cooperative Agreement

498 No.1852977. Computing and data storage resources, including the Cheyenne supercomputer
499 (doi:10.5065/D6RX99HX), were provided by the Computational and Information Systems
500 Laboratory (CISL) at NCAR. We thank all the scientists, software engineers, and administrators
501 who contributed to the development of CESM2. Previous and current CESM versions are freely
502 available at: http://www.cesm.ucar.edu/models/cesm2/. The CESM2 data analyzed in this
503 manuscript have been contributed to CMIP6 and are freely available at the Earth System Grid
504 Federation (https://esgf-node.llnl.gov/search/cmip6/) or from the NCAR Digital Asset Services
505 Hub (DASH; https://data.ucar.edu) or from the links provided from the CESM website at:
506 www.cesm.ucar.edu. The climatological snow data are available at:
507 https://doi.org/10.7265/N5MS3QNJ. The IMB data are available at: http://imb-crrel-
508 dartmouth.org. The snow radar data are available at: https://doi.org/10.5067/FAZTWP500V70,
509 processed, and made available courtesy of Dr. Ron Kwok. ATLAS/ICESat-2 L3A Sea Ice
510 Freeboard, Version 2 (ATL10) are publicly available at: https://nsidc.org/data/ATL10/versions/2.
511 Sea ice concentration data are publicly available from the Sea Ice Index Version 3 at:
512 https://nsidc.org/data/G02135/versions/3. M.A.W. conducted this work under the National
513 Aeronautics and Space Administration's New Investigator Program in Earth Science
514 (80NSSC20K0658). M.M.H. acknowledges funding from NSF (OPP 1724748). A.K.D. and
515 D.A.B. acknowledge support from the Cooperative Agreement award under NSF (1852977).

516

517 **References**

518 Bintanja, R. & Andry, O. (2017). Towards a rain- dominated Arctic. *Nat. Clim. Chang.* 7, 263–
519 267.

520

521 Blanchard-Wrigglesworth, E., S. L. Farrell, T. Newman, and C. M. Bitz (2015), Snow cover on
522 Arctic sea ice in observations and an Earth System Model, *Geophys. Res. Lett.,* 42, 10,342–
523 10,348, doi:10.1002/2015GL066049.
524
525 Danabasoglu, G., Lamarque, J. F., Bachmeister, J., Bailey, D. A., DuVivier, A. K., Edwards, J.,
526 Emmons, L. K., Fasullo, J., Garcia, R., Gettelman, A., Hannay, C., Holland, M. M., et al. (2020),
527 The Community Earth System Model version 2 (CESM2), *Journal of Advances in Modeling*
528 *Earth Systems,* 12, doi:10.1029/2019MS001916.
529
530 DeRepentigny, P., Jahn, A., Holland, M. M., and A. Smith (submitted). Arctic sea ice in the two
531 Community Earth System Model version 2 (CESM2) configurations during the 20th and 21st
532 centuries, *J. Geophys. Res. Oceans.*
533
534 DuVivier, A. K., Holland, M. M., Kay, J. E., Tilmes, S., Gettelman, A., & Bailey, D.
535 (submitted). Arctic and Antarctic sea ice state in the Community Earth System Model Version 2.
536 *Journal of Geophysical Research: Oceans.*
537
538 Fetterer, F., K. Knowles, W. N. Meier, M. Savoie, and A. K. Windnagel. 2017, updated daily.
539 Sea Ice Index, Version 3. Boulder, Colorado USA. NSIDC: National Snow and Ice Data Center.
540 doi: https://doi.org/10.7265/N5K072F8. (Accessed January 20, 2020).
541

Gettelman, A., et al. (2019). The Whole Atmosphere Community Climate Model Version 6 (WACCM6). *Journal of Geophysical Research: Atmospheres.* doi: https://doi.org/10.1029/2019JD030943

Hezel, P. J., X. Zhang, C. M. Bitz, B. P. Kelly, and F. Massonnet (2012), Projected decline in spring snow depth on Arctic sea ice caused by progressively later autumn open ocean freeze-up this century, *Geophys. Res. Lett.,* 39, L17505, doi:10.1029/2012GL052794.

Holland, M. M., J. Finnis, A. P. Barrett, and M. C. Serreze (2007), Projected changes in Arctic Ocean freshwater budgets, J. Geophys. Res., 112, G04S55, doi:10.1029/2006JG000354.

Holland, M.M. and L. Landrum (2015) Factors affecting projected Arctic surface shortwave heating and albedo change in coupled climate models, *Phil. Trans. R. Soc. A,* 373:20140162, doi:10.1098/rsta.2014.0162.

Holland, M.M., Bailey, D.A., Briegleb, B.P., Light, B., and E. Hunke (2012), Improved sea ice shortwave radiation physics in CCSM4: the impact of melt ponds and aerosols on arctic sea ice. *J. Clim.* 25, 1413–1430.

Hunke, E. C., and J. K. Dukowicz (2002), The elastic–viscous–plastic sea ice dynamics model in general orthogonal curvilinear coordinates on a sphere—Incorporation of metric terms. *Mon. Wea. Rev.,* 130, 1848–1865.

565 Hunke, E. C., and W. H. Lipscomb (2008), CICE: The Los Alamos sea ice model,
566 documentation and software, version 4.0. Los Alamos National Laboratory Tech. Rep. LA-CC-
567 06-012, 76 pp.
568
569 Hunke, E. C., Hebert, D. A., & Lecomte, O. (2013). Level-ice melt ponds in the Los Alamos sea
570 ice model, CICE. *Ocean Modelling,* 71 , 26, 42,
571 doi:https://doi.org/10.1016/j.ocemod.2012.11.008.
572
573 Hunke, E. C., Lipscomb, W. H., Turner, A. K., Jeery, N., & Elliot, S. (2015). CICE: The Los
574 Alamos Sea Ice Model Documentation and Software Users Manual Version 5.1 (Tech. Rep. No.
575 LA-CC-06-012). Los Alamos National Laboratory.
576
577 Hurrell, J. W., M. Holland, P. Gent, S. Ghan, J. E. Kay, P. Kushner, J.-F. Lamarque, W. Large,
578 D. Lawrence, and K. Lindsay (2013), The community earth system model: A framework for
579 collaborative research, *Bull. Am. Meteorol. Soc.*, 94, 1339–1360.
580
581 Kay, J. E., et al. (2015), The Community Earth System model (CESM) large ensemble project: A
582 community resource for studying climate change in the presence of internal climate variability,
583 *Bull. Am. Meteorol. Soc.,* doi:10.1175/BAMS-D-13-00255.1.
584
585 Koenig, L., Martin, S., Studinger, M. and J. Sonntag (2010), Polar airborne observations fill gap
586 in satellite data. *Eos* 91, 333–334.
587

588 Kurtz, N., and S. Farrell (2011), Large-scale surveys of snow depth on Arctic sea ice from
589 Operation IceBridge, *Geophys. Res. Lett.*, 38, L20505, doi:10.1029/2011GL049216.
590
591 Kwok, R., B. Panzer, C. Leuschen, S. Pang, T. Markus, B. Holt, and S. Gogineni (2011),
592 Airborne surveys of snow depth over Arctic sea ice, *J. Geophys. Res.*, 116, C11018,
593 doi:10.1029/2011JC007371.
594
595 Kwok, R., G. Cunningham, T. Markus, D. Hancock, J. H. Morison, S. P. Palm, S. L. Farrell, A.
596 Ivanoff, J. Wimert, and the ICESat-2 Science Team (2019), ATLAS/ICESat-2 L3A Sea Ice
597 Freeboard, Version 2. Boulder, Colorado USA. NSIDC: National Snow and Ice Data Center. doi:
598 https://doi.org/10.5067/ATLAS/ATL10.002. (Accessed January 20, 2020).
599
600 Kwok, R., Kacimi, S., Webster, M.A., Kurtz, N.T., and A.A. Petty (2020), Arctic snow depth
601 and sea ice thickness from ICESat-2 and CryoSat-2 freeboards: a first examination, *J. Geophys.*
602 *Res. Oceans*, 125, 3, https://doi.org/10.1029/2019JC016008.
603
604 Kwok, R., Cunningham, G.F., Kacimi, S., Webster, M.A., Kurtz, N.T, and A. Petty (submitted),
605 Decay of the snow cover over Arctic sea ice from ICESat-2 acquisitions during summer melt in
606 2019, submitted to *Geophys. Res. Lett.*
607
608 Light, B., S. Dickinson, D. K. Perovich, and M. M. Holland (2015), Evolution of summer Arctic
609 sea ice albedo in CCSM4 simulations: Episodic summer snowfall and frozen summers, *J.*
610 *Geophys. Res. Oceans,* 120, 284–303, doi:10.1002/2014JC010149.

Lique, C., Holland, M. M., Dibike, Y. B., Lawrence, D. M. & Screen, J. A. (2016). Modeling the Arctic freshwater system and its integration in the global system: Lessons learned and future challenges. *J. Geophys. Res. Biogeosci.*, 121, 540–566.

Maykut, G. A. (1978), Energy exchange over young sea ice in the central Arctic, *J. Geophys. Res.*, 83, 8C0241, doi:10.1029/JC083iC07p03646.

McIlhattan, E. A., T. S. L'Ecuyer, and N. B. Miller (2017), Observational evidence linking arctic supercooled liquid cloud biases in CESM to snowfall processes, *J. Clim.*, doi:10.1175/JCLI-D-16-0666.1.

McIlhattan, E. A., Kay, J. E., & LEcuyer, T. S. (submitted). Arctic Clouds and Precipitation in the Community Earth System Model Version 2. Journal of Geophysical Research: manuscript submitted to *JGR: Oceans Atmospheres.*

Meehl, G. A., et al. (submitted), Characteristics of Future Warmer Base States in CESM2, *Journal of Advances in Modeling Earth Systems.*

Nandan, V. et al. (2017), Effect of snow salinity on CryoSat-2 Arctic first-year sea ice freeboard measurements. *Geophys. Res. Lett.* 44, 10419–10426.

O'Neill, B. C., Tebaldi, C., van Vuuren, D. P., Eyring, V., Friedlingstein, P., Hurtt, G., et al. (2016). The Scenario Model Intercomparison Project (ScenarioMIP) for CMIP6. *Geosci. Model Dev.*, 9, 3461–3482, 2016, doi:10.5194/gmd-9-3461-2016

Panzer, B., C. Leuschen, A. Patel, T. Markus, and S. Gogineni (2010), Ultrawideband radar measurements of thickness of snow over sea ice, *IEEE Trans. Geosci. Remote Sens.*, 45, 2715–2724, doi:10.1109/IGARSS.2010.5654342.

Perovich, D. K., T. C. Grenfell, B. Light, and P. V. Hobbs (2002), Seasonal evolution of the albedo of multiyear Arctic sea ice, *J. Geophys. Res.*, 107(C10), 8044, doi:10.1029/2000JC000438.

Perovich, D. K., and C. Polashenski (2012), Albedo evolution of seasonal Arctic sea ice, *Geophys. Res. Lett.*, 39, L08501, doi:10.1029/2012GL051432.

Perovich, D., C. Polashenski, A. Arntsen, and C. Stwertka (2017a), Anatomy of a late spring snowfall on sea ice, *Geophys. Res. Lett.*, 44, 2802–2809, doi:10.1002/2016GL071470.

Perovich, D. et al. (2017b) Observing and understanding climate change: Monitoring the mass balance, motion, and thickness of Arctic sea ice. http://imb-crreldartmouth.org.

Petrich, C., H. Eicken, C. M. Polashenski, M. Sturm, J. P. Harbeck, D. K. Perovich, and D. C. Finnegan (2012), Snow dunes: A controlling factor of melt pond distribution on Arctic sea ice, *J. Geophys. Res.*, 117, C09029, doi:10.1029/2012JC008192.

Provost, C. et al. (2017). Observations of flooding and snow-ice formation in a thinner Arctic sea-ice regime during the N-ICE2015 campaign: influence of basal ice melt and storms. *J. Geophys. Res. Oceans* 122, 7115–7134.

Radionov, V. F., N. N. Bryazgin, and E. I. Alexandrov (1997), The Snow cover of the Arctic Basin, Tech. Rep. APL-UW-TR 9701, 95 pp., Appl. Phys. Lab., Univ. of Wash., Seattle, Wash.

Sturm, M. & Massom, R. A. (2017) in Sea Ice 3rd edn (ed. Thomas, D. N.) 65–109 (Wiley and Blackwell, Oxford).

Sturm, M., D. K. Perovich, and J. Holmgren (2002), Thermal conductivity and heat transfer through the snow on the ice of the Beaufort Sea, *J. Geophys. Res.*, 107(C21), 8043, doi:10.1029/2000JC000409.

Turner, A. K., E. C. Hunke, and C. M. Bitz (2013), Two modes of sea-ice gravity drainage: A parametrization for large-scale modeling, *J. Geophys. Res.*, doi:10.1002/jgrc.20171.

van Vuuren, D. P., Edmonds, J., Thomson, A., Riahi, K., Kainuma, M., Matsui, T., Hurtt, G. C., Lamarque, J.-F., Meinshausen, M., Smith, S., Granier, C., Rose, S. K., and Hibbard, K. A.: The Representative Concentration Pathways: an overview, *Climatic Change*, 109, 5–31, 2011

Warren, S. G. et al. (1999). Snow depth on Arctic sea ice. *J. Clim.* 12, 1814–1829.

Webster, M. A. et al. (2014). Interdecadal changes in snow depth on Arctic sea ice. *J. Geophys. Res. Oceans* 119, 5395–5406.

Webster, M. A., I. G. Rigor, D. K. Perovich, J. A. Richter-Menge, C. M. Polashenski, and B. Light (2015), Seasonal evolution of melt ponds on Arctic sea ice, *J. Geophys. Res. Oceans*, 120, 5968–5982, doi:10.1002/2015JC011030.

Webster, M. A. et al. (2018). Snow in the changing sea-ice systems. *Nat. Clim. Chang.* 8, 946–953.

Webster, M. A., Parker, C., Boisvert, L., & Kwok, R. (2019). The role of cyclone activity in snow accumulation on Arctic sea ice. *Nat. Comm.*, 10(1), 5285. https://doi.org/10.1038/s41467-019-13299-8

695 **Tables**

696 **Table 1.** The number of ensemble members from each model configuration used in the analysis.
697 We note that for the SSP3-7.0 experiment using CESM2-WACCM6, model ensemble members
698 2 and 3 stop in year 2055.

	Historical	SSP1-2.6	SSP2-4.5	SSP3-7.0	SSP5-8.5	RCP 8.5
CESM-LE	30	-	-	-	-	30
CESM2-CAM6	11	2	3	6	2	-
CESM2-WACCM6	3	1	5	3	5	-

699

700 **Table 2.** The temporal and spatial information of each "observational" data set analyzed in the
701 analysis.

	Temporal Coverage	Temporal Resolution	Spatial Resolution
North Pole Ice Stations	1954-1991	Every 10 days	10 m
Ice Mass Balance Buoys	1997-2017	Daily	Point measurement
Operation IceBridge	2009-2017	Every spring	40 m
ICESat-2	2018-2019	Monthly	25 km

702

703

704

705

706

Figures

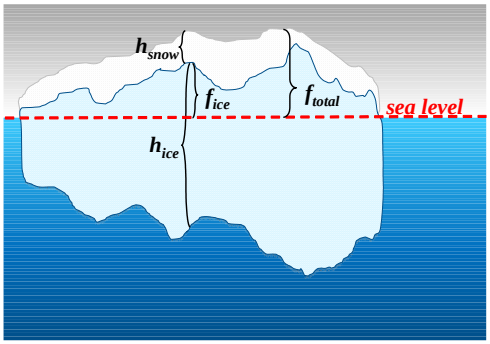

Figure 1. A schematic showing the relationship between snow depth, sea ice freeboard, sea ice thickness, and total (snow and sea ice) freeboard as shown in Equation 1.

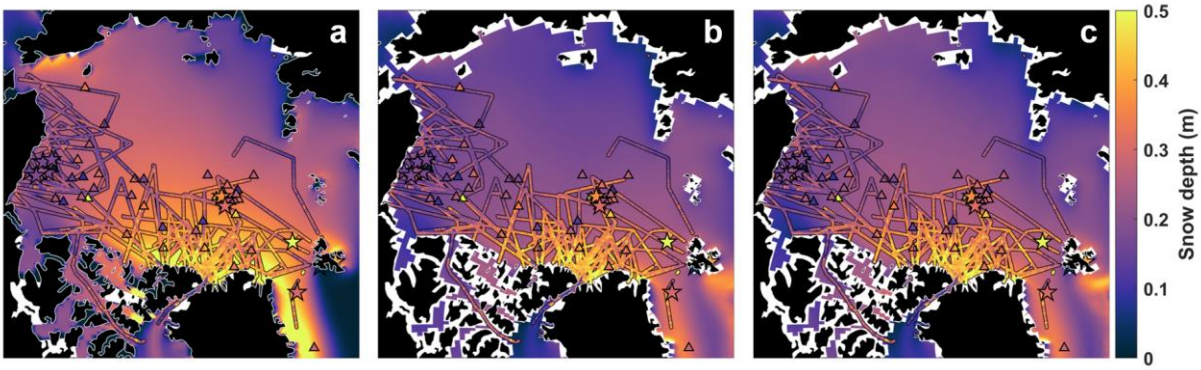

Figure 2. The 2000-2017 modeled spring (March-April) snow depth distributions with ground, buoy, and airborne observations overlaid from the 2000-2017 period. The model results are from: (a) CESM-LE; (b) CESM2-CAM6; and (c) CESM2-WACCM6.

716

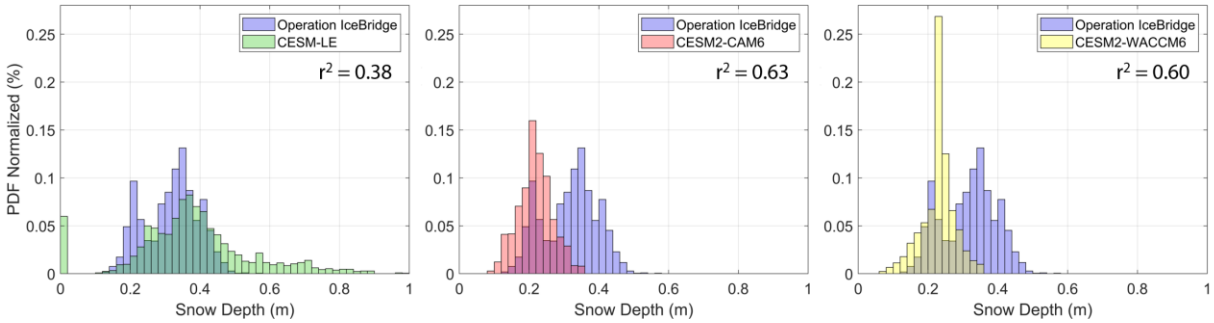

717

718 **Figure 3.** A comparison of 2009-2017 spring (March-April) snow depth distributions between
719 Operation IceBridge and modeled data. (a) snow depth distributions retrieved by airborne radar
720 compared to those simulated by CESM-LE; (b) the same as in (a) comparing radar retrievals and
721 CESM2-CAM6 snow depth distributions; and (c) the same as (a) comparing radar retrievals and
722 CESM2-WACCM6 snow depth distributions. Correlation coefficients were statistically
723 significant to the 99%. The bin width is 2 cm.

724

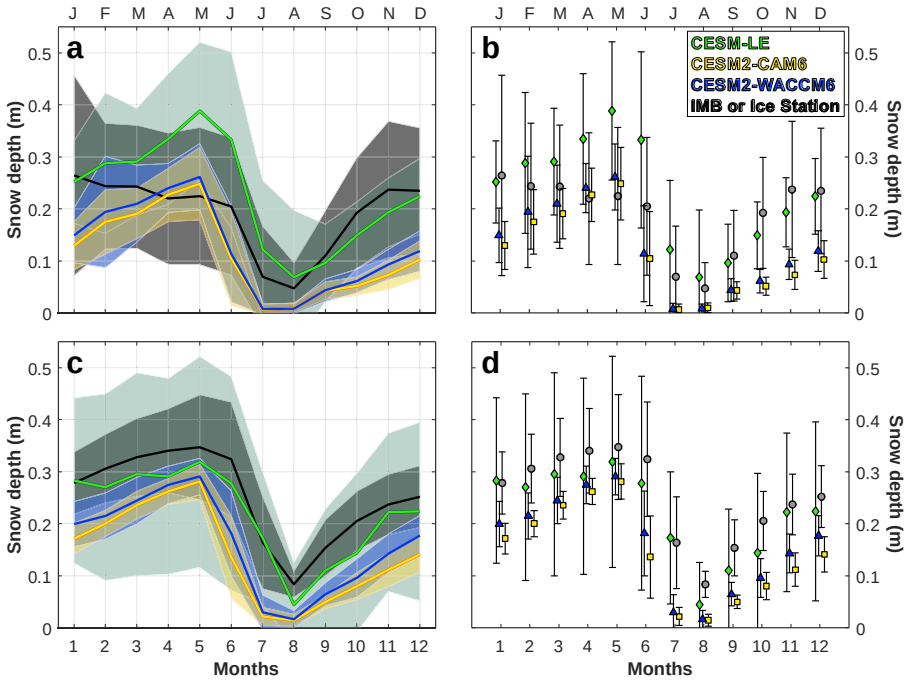

725

Figure 4. (a) and (b) show the mean (solid) and standard deviation (spread and bars) in snow depth for IMBs and CESM configurations for each month at all IMB locations. The squared correlation coefficients were 0.09, 0.11, and 0.12 for CESM-LE, CESM2-CAM6, and CESM2-WACCM6, respectively. Panels (c) and (d) show the mean (solid) and standard deviation (spread and bars) in snow depth for the survey lines at the drifting ice stations and CESM for each month at all station locations. The squared correlation coefficients were 0.16, 0.49 and 0.53 for CESM-LE, CESM2-CAM6, and CESM2-WACCM6, respectively.

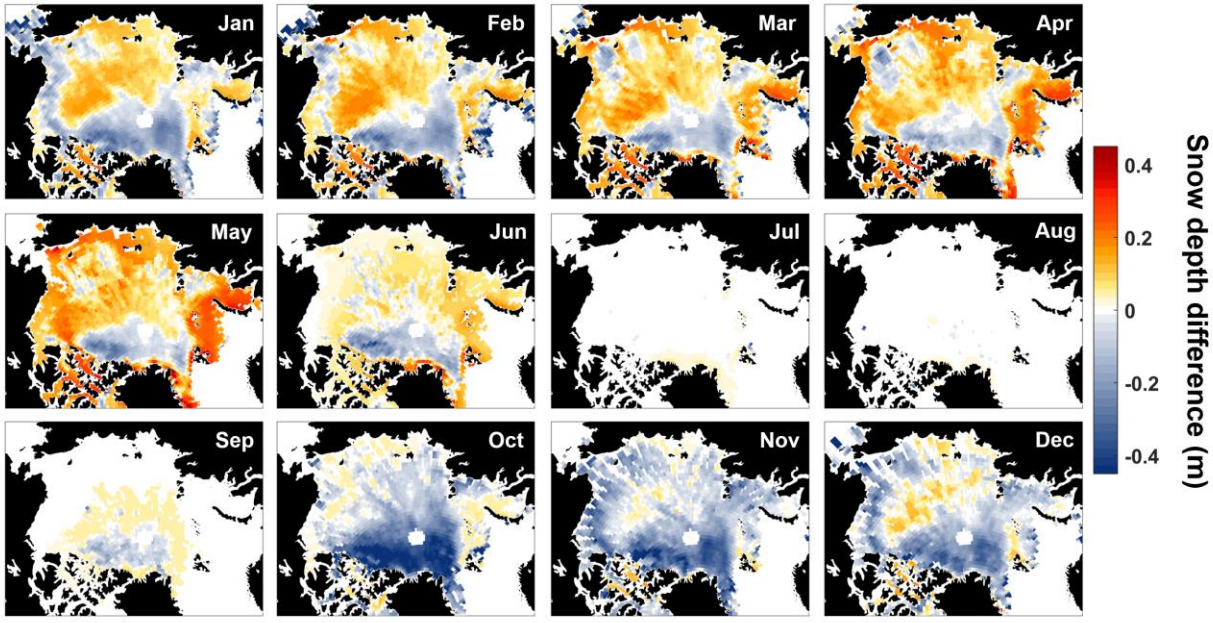

Figure 5. The difference in snow depth directly available from CESM2-WACCM6 minus that derived from ICESat-2 data (using CESM snow depth and sea ice thickness). The CESM2-WACCM6 data were averaged over 2010-2019, while the ICESat-2 data are available for 2018-2019.

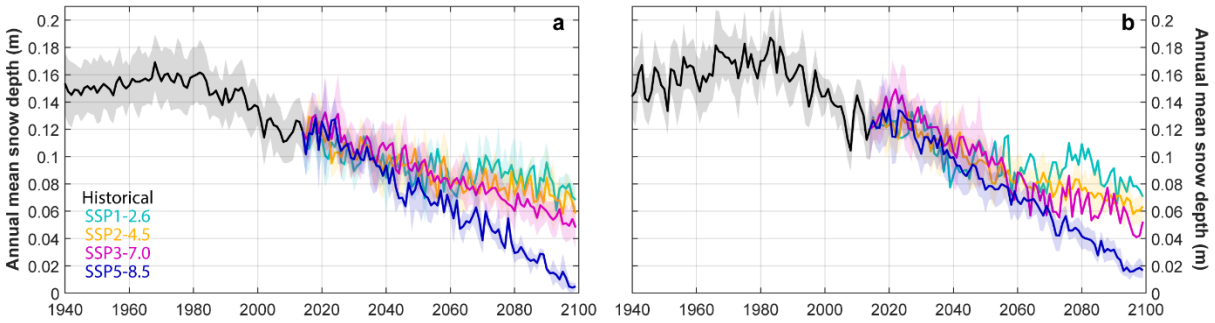

Figure 6. Projections of annual mean snow depth over 80-90ºN under different forcing scenarios for (a) CESM2-CAM6 and (b) CESM2-WACCM6. The solid lines represent the model ensemble mean, while the spread is the standard deviation among ensemble members. Please note the differences in y-axis scales and that the spread, or lack thereof, is largely due to the number of available ensemble members (see Table 1).

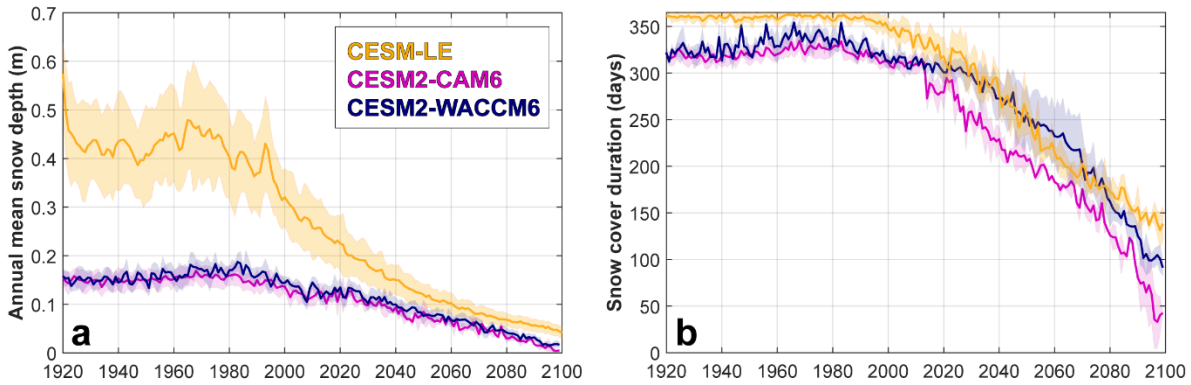

Figure 7. (a) The annual mean snow depth at 80-90ºN for historical models runs and projected under the SSP5-8.5 and RCP8.5 forcing scenario for CESM2 and CESM-LE, respectively; and (b) the number of days (duration) with at least 0.01 m snow depth and 15% sea ice concentration over 80-90ºN for historical models runs and projected under the SSP5-8.5/RCP8.5 forcing scenario. The spread in both panels is the standard deviation across model ensemble members,

753 while the solid line is the ensemble mean. Note, the number of ensemble members changed from
754 11 to two for CESM2-CAM6 and three to five for CESM2-WACCM6 in 2015, which affects the
755 spread.
756

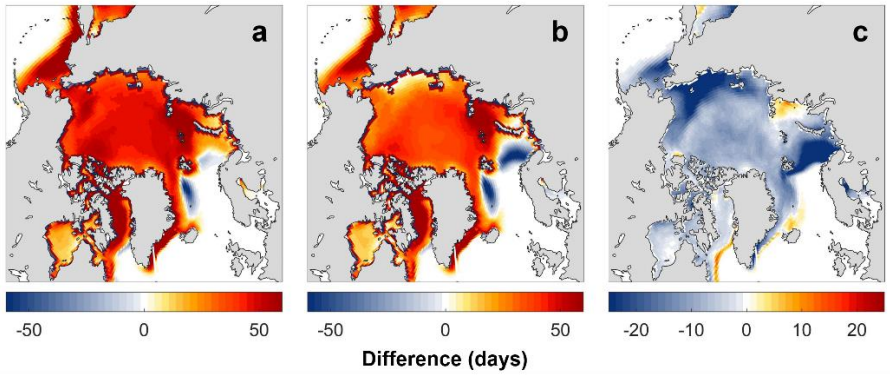

757

758 **Figure 8.** The difference in the snow cover duration, defined as the number of days when the
759 snow cover was at least 0.01 m thick and sea ice concentration at least 15%, for (a) CESM-LE
760 minus CESM2-CAM6, (b) CESM-LE minus CESM2-WACCM6, and (c) CESM2-CAM6 minus
761 CESM2-WACCM6.
762

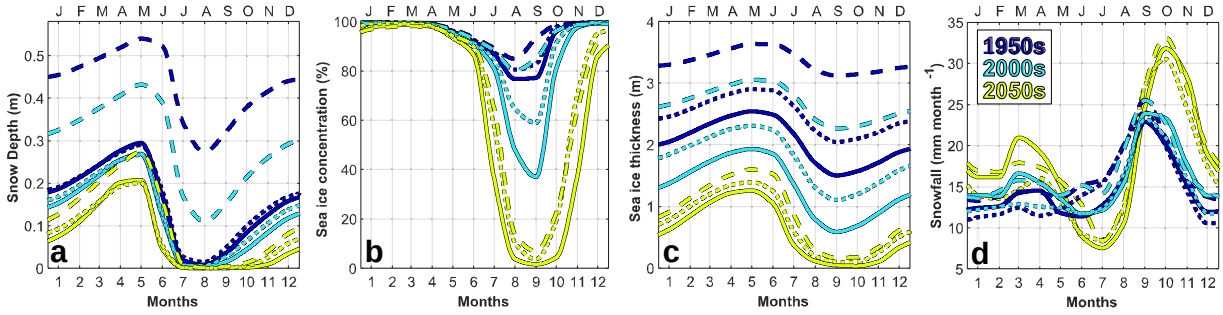

763

764 **Figure 9.** Decadal averages of (a) snow depth, (b) sea ice concentration, (c) sea ice thickness,
765 and (d) snowfall over 80ºN-90ºN for the 1950s, 2000s, and 2050s from CESM-LE (dashed),
766 CESM2-CAM6 (solid) and CESM2-WACCM6 (dotted) under the RCP8.5 and SSP5-8.5 forcing
767 scenarios.

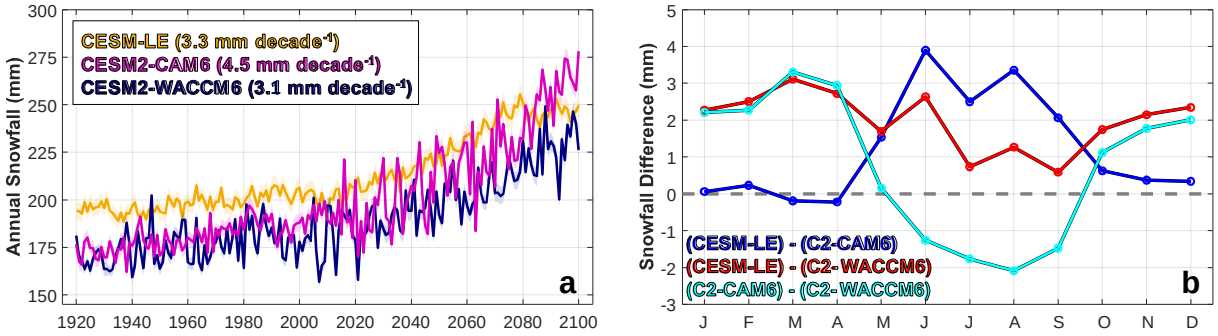

Figure 10. (a) The annual snowfall over 80ºN-90ºN for all model configurations from 1920 to 2100 under the RCP 8.5 and SSP5-8.5 forcing scenarios; (b) The difference between model configurations in monthly mean snowfall averaged over 1920-2100 and 80ºN-90ºN under the same forcing scenarios as panel (a).

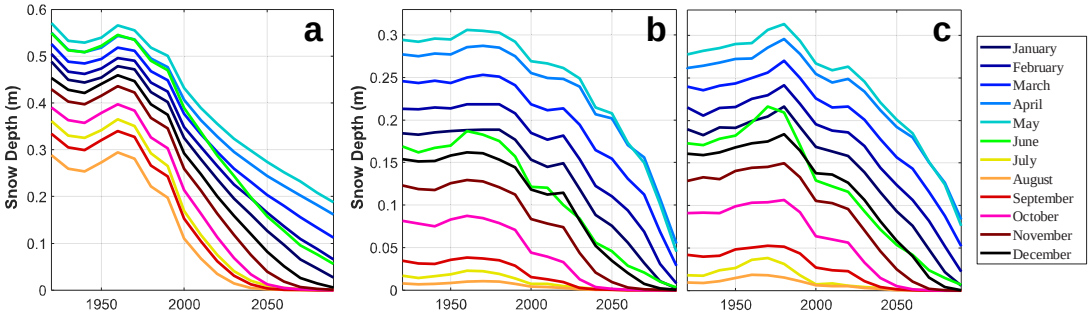

Figure 11. Mean monthly snow depths over 80ºN-90ºN for (a) CESM-LE (b) CESM2-CAM6, and (c) CESM2-WACCM6 under the RCP8.5 and SSP5-8.5 forcing scenarios. Note the scale change between panel (a) and panels (b – c) to better illustrate the large snow depths in CESM-LE.

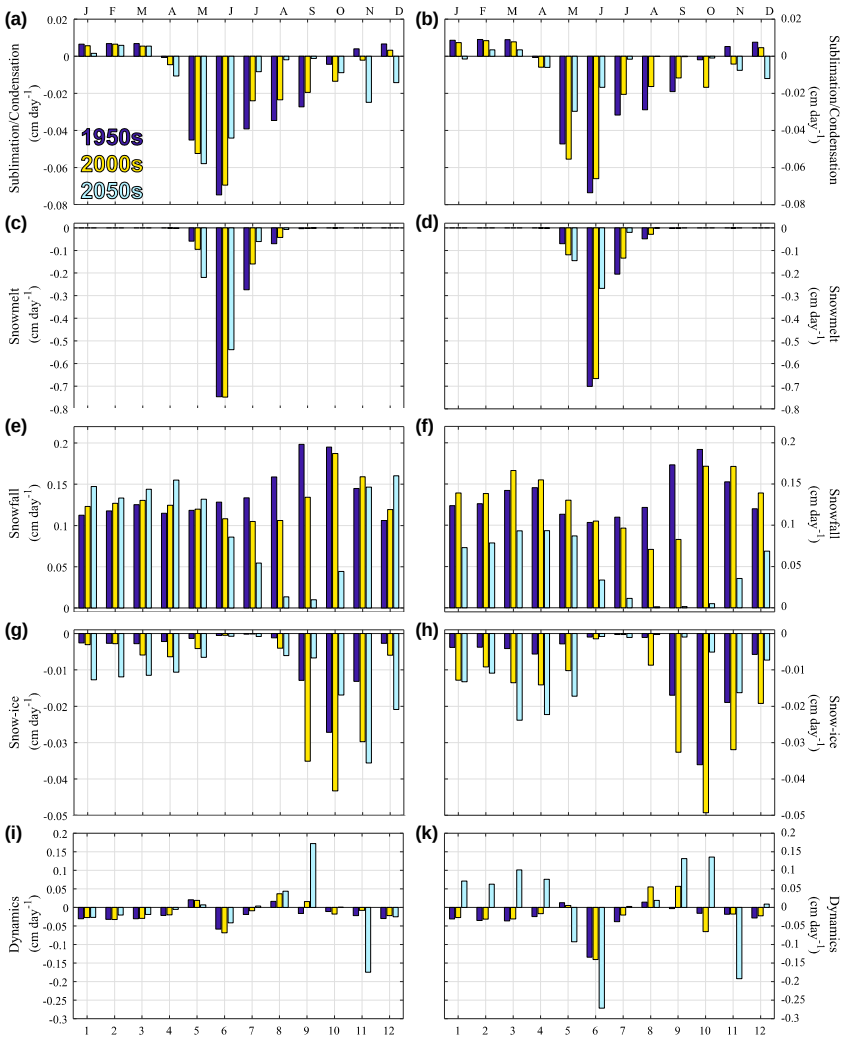

781

782 **Figure 12.** Decadal averages from (left) CESM2-WACCM6 and (right) CESM2-CAM6 of snow
783 processes that constitute the snow mass budget over the annual cycle. Averages are taken over
784 80ºN-90ºN for the 1950s, 2000s, and 2050s under the SSP5-8.5 forcing scenario. The snow
785 processes include: (a-b) sublimation and condensation, (c-d) snowmelt, (e-f) accumulation from
786 snowfall, (g-h) snow-ice formation, and (i-k) dynamics.

787

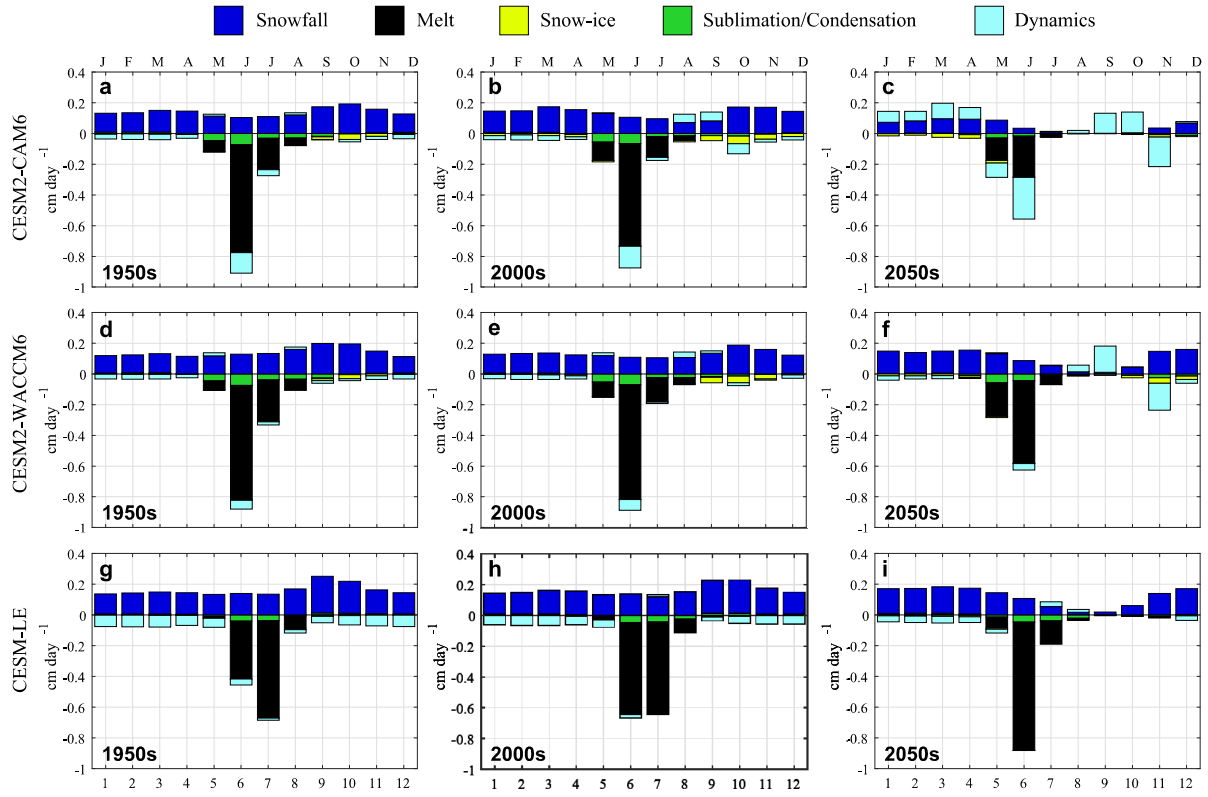

788

789 **Figure 13.** Snow processes that comprise the snow mass budget for (a-c) CESM2-CAM6, (d-f)

790 CESM2-WACCM6, and (g-i) CESM-LE. The decadal averages for 1950s, 2000s, and 2050s

791 over 80ºN-90ºN are shown. Note the scale change for panels g-i.

792

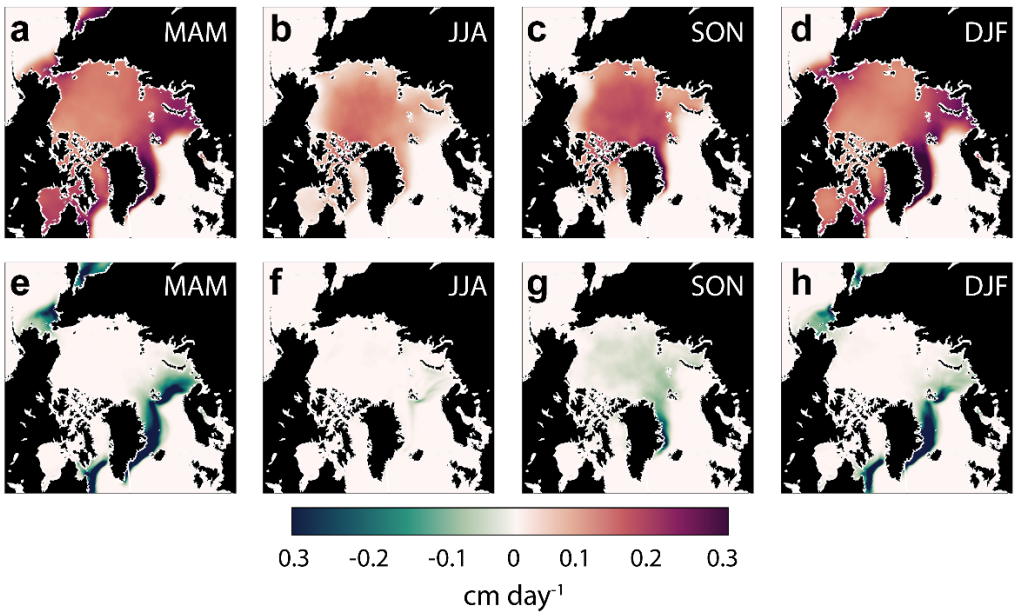

Figure 14. The 2000-2009 average (a-d) snow mass gain from snowfall and (e-h) snow mass loss from snow-ice formation for each season in CESM2-WACCM6.